Comparison study of dimensionally stable anodes for degradation of chlorpyrifos in water

Gayani Chathurika Pathiraja[1], Pavithra Bhakthi Jayathilaka[1], Chandima Weerakkody[1], Parakrama Karunarathne[2] and Nadeeshani Nanayakkara[1,3,*]

[1]Environmental Engineering/Electrochemistry Research Group, Institute of Fundamental Studies, Hantana Road, Kandy, Sri Lanka
[2]Department of Chemical and Process Engineering and [3]Department of Civil Engineering, Faculty of Engineering, University of Peradeniya, Sri Lanka

In the present study, two dimensionally stable anodes, Ti/IrO_2 and Ti/IrO_2–SnO_2, have been developed in order to degrade chlorpyrifos in chloride-free environment. The chemical oxygen demand (COD) results revealed that Ti/IrO_2–SnO_2 electrode had degraded 78.2% of COD after 6 h of electrolysis. COD removal followed pseudo second-order kinetics. Radical scavenger studies confirmed that the hydroxyl radical can be the major factor responsible for degrading chlorpyrifos. The anodic charge decreased from 153.76 to 145.15 mC while accelerated lifetime showed 7 h increment, indicating the higher stability of Ti/IrO_2–SnO_2 anode. The qualitative identification of oxides of both electrodes was studied by X-ray diffraction. Roughness parameters and topography were determined using AFM images.

Keywords: Chlorpyrifos, chloride free environment, dimensionally stable anode.

PESTICIDES have been recognized as one of the major organic pollutants in water streams because of their increasing use in agriculture. Chlorpyrifos (0,0-diethyl-0-(3,5,6-trichloro-2-pyridinyl) phosphorothioate) is one of the most widely used organophosphate pesticides in agricultural pest control and in households as a termiticide. It is recognized as one of the top five commercial insecticides due to its broad-spectrum effectiveness, flexibility for use in multiple delivery systems and relatively short persistence. Excessive exposure to chlorpyrifos and its metabolites may cause poisoning. Acute poisoning may result in headache, nausea, muscle twitching, and in extreme cases even death. It affects the central nervous system, cardiovascular system and respiratory system. In addition, it acts as a skin and eye irritant[1]. As a consequence, the use of chlorpyrifos has been vastly restricted in the United States and in some European countries. However, excessive and continuous use of chlorpyrifos has led to detection of its residues in surface water, groundwater and soil in many countries[2–4]. It should be noted that the guideline value for chlorpyrifos in drinking water, as set by the World Health Organization is 30 μg/l (ref. 5). Moreover, tolerances for chlorpyrifos in raw agricultural commodities, foods and animal feeds have been established by the US Environmental Protection Agency ranging from 0.05 to 25 ppm (ref. 6). As such, treating chlorpyrifos-contaminated water is of high importance.

Electro-enzymatic degradation[1], microbial degradation[7], photo-Fenton oxidation[8], photo-catalytic degradation using doped polycrystalline TiO_2 (ref. 9), ultrasonic and ozone treatments[10,11], high-pressure arc discharge plasma process[12] and ionizing radiation[13] have been utilized to remove chlorpyrifos from water.

In recent years, the electrochemical degradation of organic compounds is an emerging technology due to factors such as *in situ* chemical generation, ease in process control, environmental compatibility, safety, cost-effectiveness and high efficiency[14–16]. In electrochemical degradation of organic compounds, the degradation efficiency depends highly on the anode material[15–21]. However, only limited studies have been done on using dimensionally stable anodes (DSAs) to treat chlorpyrifos in water[22]. In addition, most of the reported works on electrochemical degradation of organic pollutants are limited to efficiency studies in different experimental conditions. Moreover, those studies depend on the presence of chloride ion in the electrolyte. The present study, therefore, is related to electrochemical degradation of chlorpyrifos by developing two types of DSA (Ti/IrO_2 and Ti/IrO_2–SnO_2) electrodes. More specifically, the present study reports the efficiency in degradation of chlorpyrifos and the electrochemical properties of the developed anodes in chloride-free electrolytes. The morphological characterization of the Ti/IrO_2–SnO_2 anode before and after deactivation has been performed to reveal its stability.

Experimental

Materials

All chemicals, including chlorpyrifos (99.5%, Sigma-Aldrich), Na_2SO_4 anhydrous AR (99%, SDFCL), NaOH

*For correspondence. (e-mail: kgnn@pdn.ac.lk)

(97.5%, BDH VWR International), Na_2CO_3 (99%, BDH), RNO (Sigma-Aldrich), $H_2C_2O_4{\cdot}2H_2O$ (99%, LOBAL Chemie), HCl (37%, BDH), $IrCl_3{\cdot}3H_2O$ (Ir–53–56%, ACRDS Organics), Sn standard solution (Fisher Scientifics), ethanol (99% AR, Fisher Scientifics), isopropanol, $K_2Cr_2O_7$ (99%, Avondale Laboratories), H_2SO_4 (98%, Fisher Scientifics) and Ag_2SO_4 (Fisher Scientifics), were of analytical reagent grade. All aqueous solutions were prepared using deionized (DI) water.

Preparation of two kinds of DSA

Titanium plates with a dimension of 10 mm × 10 mm × 2.5 mm, i.e. an effective geometric area of 2.5 cm^2, were used as substrates. Prior to dip-coating, the electrode was sandblasted followed by a chemical treatment using 5% (w/w) oxalic acid solution for 10 min and 37% (w/w) HCl acid for 5 min. The substrate was then dried at 100°C until it reaches a constant weight.

The precursor solution for depositing IrO_2 was prepared by dissolving 0.56 g of $IrCl_3{\cdot}3H_2O$ in 4.6 ml ethanol[23], dip-coated, air-dried in 80°C for 5 min to allow solvents to vapourize and calcinated in an oven at 450°C for 10 min. This process was repeated until the final coating load reached 1 mg/cm^2. Finally, it was post-backed at 500°C in a muffle furnace (OT-HTMF-05, Optics Technology, Delhi) for 1 h (ref. 14).

The precursor solution for depositing IrO_2–SnO_2 coating was prepared with the support of polymeric precursor solution by dissolving 0.56 g of $IrCl_3{\cdot}3H_2O$ in 4.6 ml ethanol[23] and 1% polyethylene glycol (1000) by Ir concentration. It was dip-coated and the wet coating surface was air-dried in 80°C airflow to evaporate solvents. Then the coating layer was calcinated in an oven at 450°C for 10 min. The electrode was washed with distilled water to remove the coated polymer and make pores on the layer. The second precursor solution was prepared by dissolving 0.66 ml of Sn (1000 ppm) standard solution in 3.3 ml of isopropanol[23]. Then it was applied on the washed electrode surface. The wet coating surface was then air-dried in 80°C air flow to evaporate solvents and calcinated in an oven at 450°C for 10 min. This process was repeated to achieve the final coating load of 1 mg/cm^2. After reaching the final coating load, the electrode was post-backed at 500°C in the muffle furnace for 1 h. Triplicate samples of the electrodes were prepared in both the cases.

Electrochemical degradation of chlorpyrifos

The chemical oxygen demand (COD) was determined as an indication of the degradation of chlorpyrifos by the dichromate method[24]. The metal oxide electrodes described above as an anode and a Ti plate as a cathode, were set at a distance of 1 cm. The operating current density was 20 mA cm^{-2}. The appropriate amount of samples was collected during 6 h and absorbance was measured using UV–visible spectrophotometer (Shimadzu, UV-2450, wavelength = 600 Å). The rate constants were calculated using pseudo first-order model and pseudo second-order model.

Determination of current efficiency

The instantaneous current efficiency (ICE) for the anodic oxidation of chlorpyrifos was calculated using the following expression[25]:

$$\mathrm{ICE} = \frac{[(\mathrm{COD})_t - (\mathrm{COD})_{t+\Delta t}]FV}{8I\Delta t}, \quad (1)$$

where $(COD)_t$ and $(COD)_{t+\Delta t}$ are the initial chemical oxygen demand (gO_2 m^{-3}) at time t and $t + \Delta t(s)$ respectively, I is the applied current (A), F is the Faraday constant (C mol^{-1}) and V is the volume of the electrolyte (m^3).

Detection of $OH^{\bullet}$ radical species

The bleach of RNO during the electrochemical treatment was measured as an indication of the production of free radicals in the electrochemical cell. The electrodes described above were used as the anode (one at a time) and a Ti plate was used as the cathode. Distance between the anode and the cathode was 1 cm. The operating current density was 20 mA cm^{-2}. The bleaching of RNO in supporting electrolyte Na_2SO_4 by hydroxyl radicals was measured by absorbance changes of samples taken at time intervals of 5 or 10 min by UV–visible spectrophotometer (Shimadzu, UV-2450) at 440 nm (ref. 26).

XRD analysis

The corresponding oxides of electrodes was identified by XRD analysis with CuKα radiation (λ = 1.5406 Å) at 20 kV. The scanning rate was 2° min^{-1}.

Electrochemical measurements

Cyclic voltammetry (CV) was operated for the electrodes to evaluate electrochemical properties using potentiostat/galvanostat equipment (Autolab, PGSTAT128N) at room temperature. The electrodes under study were used as the working electrode (WE), titanium plate as the counter electrode (CE), and Ag/AgCl electrode was used as the reference electrode (RE). Range of voltage scan was from –2.5 to 2.5 V at a scan rate of 0.1 V/s. Na_2SO_4 (0.5 M) was used as the electrolyte.

Accelerated lifetime test

In order to assess the electrode stability of the prepared anodes, accelerated lifetime tests were performed under harsh conditions. The tests were conducted in a three-electrode cell, the electrodes under study were used as the WE, titanium plate as CE and Ag/AgCl electrode was used as RE. The electrolyte was 0.5 M H_2SO_4. An anodic current density of 800 mA/cm^2 was used in all the studies. Experiments were carried out at room temperature (25°C). The electrolysis time at which the anodic potential reached 2 V higher than the voltage at time zero was considered as the lifetime of the coated anode.

Results and discussion

Influence of anode composition on rate of COD removal

COD removal during the electrolysis time was studied to evaluate the COD degradation efficiency and its kinetics. The electrochemical oxidation of chlorpyrifos was carried out with Ti/IrO_2 and Ti/IrO_2–SnO_2 as anodes in Na_2SO_4 electrolyte. Figure 1 shows the variation of COD removal with electrolysis time, degrading 1 mg/l of chlorpyrifos at current density of 20 mA/cm^2. It was found that when using the prepared Ti/IrO_2–SnO_2 electrode as an anode, 78.2% of COD removal efficiency can be achieved after the electrolysis time of 6 h in comparison to 65.1% of COD removal obtained with Ti/IrO_2 electrode. From these results, it can be concluded that there is a significant increment in COD removal efficiency when using Ti/IrO_2–SnO_2 electrode compared to Ti/IrO_2 electrode.

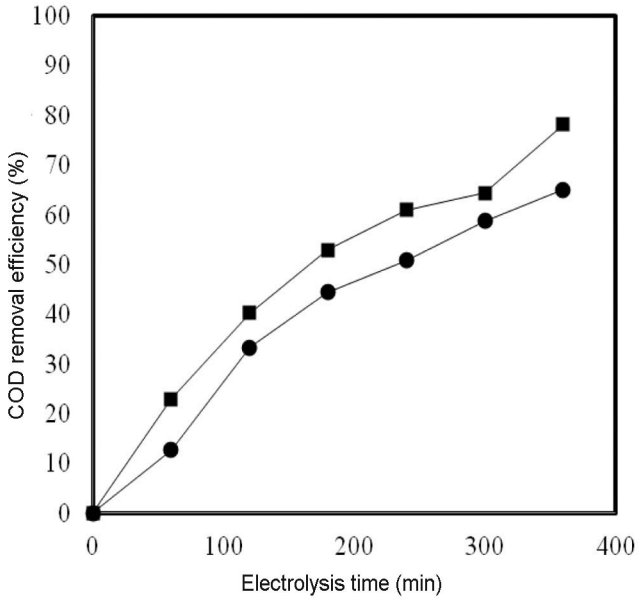

Figure 1. Variation of COD removal efficiency with electrolysis time for different anodes in Na_2SO_4 electrolyte. (●) Ti/IrO_2, (■) Ti/IrO_2–SnO_2; current density = 20 mA/cm^2, reaction time = 6 h; chlorpyrifos = 1 mg/l and temperature = 25°C.

The pseudofirst-order rate constant and pseudosecond-order rate constant (K') were calculated for the two types of electrodes at room temperature; the results are shown in Table 1. It is assumed that the hydroxyl radical concentration is a constant during the electrolysis. Then the COD removal rate r can be expressed as follows[22]:

$$r = -\frac{\mathrm{dCOD}}{\mathrm{d}t} = k[\mathrm{HO}^0]^{\alpha}\,\mathrm{COD}^2(t) = K_{\mathrm{app}}\mathrm{COD}^2(t), \qquad (2)$$

where α is the reaction order related to the hydroxyl radicals, k is the real rate constant and k_{app} is the global apparent rate constant for COD removal. Integrating this with initial COD concentration leads to a straight line whose slope represents k_{app} of the reaction.

$$\frac{1}{\mathrm{COD}(t)} - \frac{1}{\mathrm{COD}(0)} = k_{\mathrm{app}} \cdot t. \qquad (3)$$

Table 1 indicates that the pseudosecond-order model has higher regression coefficients (R^2) than the pseudo first-order model. As a consequence, the former model may give better prediction. Moreover, several authors have reported that COD of organic molecules can be followed using pseudosecond-order kinetics when they are degraded by electrochemical methods[22,27,28]. Samet *et al.*[22] suggested that it can be related to the chlorpyrifos-oxon and 3,5,6 trichloropyridinol (TCP), which are the main, stable initial byproducts of chlorpyrifos degradation[22].

Moreover, as clearly seen, k_{app} of Ti/IrO_2–SnO_2 has a high value, compared to Ti/IrO_2 electrode. It implies that Ti/IrO_2–SnO_2 electrode generates more oxygen at the electrode surface and eventually mass transport is significantly high. This is accompanied by more chlorpyrifos molecules towards the anode surface, resulting a high value of k_{app}. These findings are in good agreement with the electrochemical oxidation of chlorpyrifos using PbO_2 anode, as a function of different apparent current densities[22].

The electrochemical oxidation of chlorpyrifos was carried out with two electrolytes (Figure 2). Na_2CO_3 was

Table 1. Regression coefficients (R^2) and global apparent rate constant (k_{app}) for chemical oxygen demand removal of Ti/IrO_2 and Ti/IrO_2–SnO_2 electrodes

Electrode	Ti/IrO_2	Ti/IrO_2–SnO_2
First-order (R^2)	0.956	0.944
Second-order (R^2)	0.977	0.989
$k_{\mathrm{app}} \times 10^4$ (L/(mg min))	0.228	0.244

used as the $OH^{\bullet}$ radical scavenger[29]. The removal efficiency was found to decrease in Na_2CO_3, it decreased further with double the concentration of Na_2CO_3. As such, it is clear that the $OH^{\bullet}$ radical is generated in Na_2SO_4 electrolyte and the generated radical is scavenged by Na_2CO_3 reducing the removal efficiency.

Current efficiency with electrolysis time for different anodes

The ICEs of the electrodes in COD degradation were determined. Figure 3 shows a considerable difference in ICE of the two anodes. It can be observed that when the $Ti/IrO_2–SnO_2$ electrode is used as an anode, the ICE value is always higher during the period of reaction under similar conditions. Obviously, $Ti/IrO_2–SnO_2$ electrode is more active.

However, for both anodes, the value of ICE was relatively higher at the initial period of reaction, and then decreased dramatically with increase in electrolysis time. The influence of better mass transfer at higher initial COD concentration can be a reason for this behaviour[30]. In addition, the higher activity and stability of the anode during initial reaction hours may have influenced the variation as well.

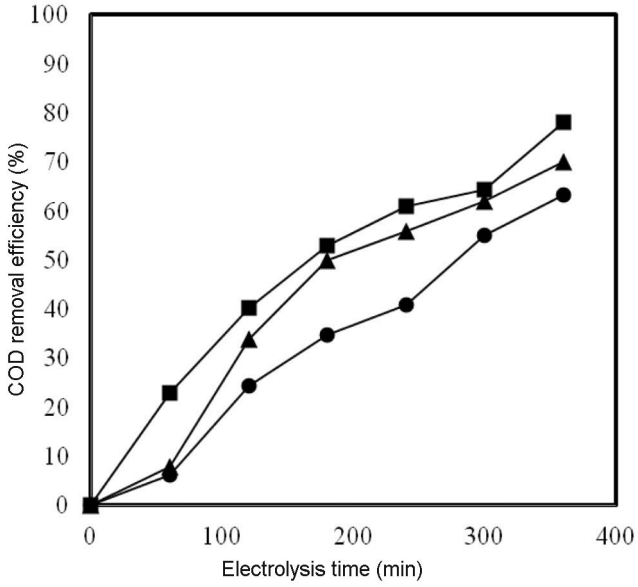

Figure 2. Variation of COD removal percentage with electrolysis time for $Ti/IrO_2–SnO_2$ electrode with different electrolytes. (■) 10 g/l of Na_2SO_4; (▲) 10 g/l of Na_2CO_3; (●) 20 g/l of Na_2CO_3; current density = 20 mA/cm^2, reaction time = 6 h, chlorpyrifos = 1 mg/l and temperature = 25°C.

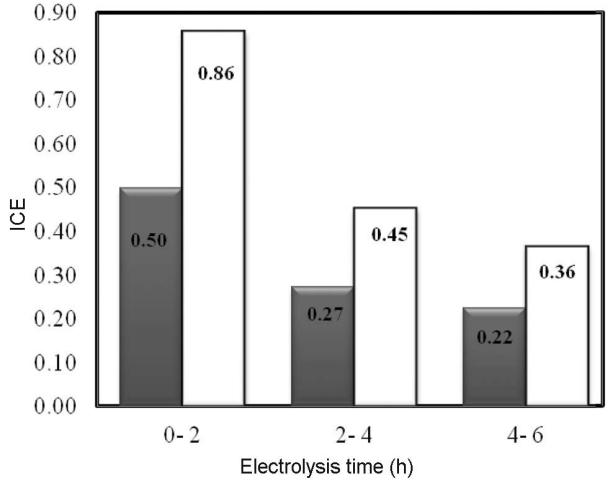

Figure 3. Change in instantaneous current efficiency with respect to electrolysis time of electrodes for the degradation of 1 mg/l chlorpyrifos solution. (■) Ti/IrO_2; (□) $Ti/IrO_2–SnO_2$; electrolyte = 10 g/l of Na_2SO_4; current density = 20 mA/cm^2; reaction time = 6 h.

Generation of $OH^{\bullet}$ radical at different anodes

The selective reaction between RNO and hydroxyl radicals was used to determine the generation of hydroxyl radicals at the two anodes. Figure 4 shows that the absorbance of RNO decreases rapidly in the initial 35 min for both anodes. The bleaching ratios of RNO at $Ti/IrO_2–SnO_2$ and Ti/IrO_2 anodes were 89.4% and 87.3% respectively. As such, it is clear that the rate of bleaching of RNO on $Ti/IrO_2–SnO_2$ anode is slightly higher compared to that of the Ti/IrO_2 anode. Therefore, it shows that bleaching successfully occurred at both anodes and the hydroxyl radical was produced at both anodes. Thus, hydroxyl radical may have played a crucial role in degrading chlorpyrifos in chloride-free environment. In addition, it can be said that the electrocatalytic activity of SnO_2 may have enhanced the efficiency of chlorpyrifos degradation, while IrO_2 coating layer was indispensable.

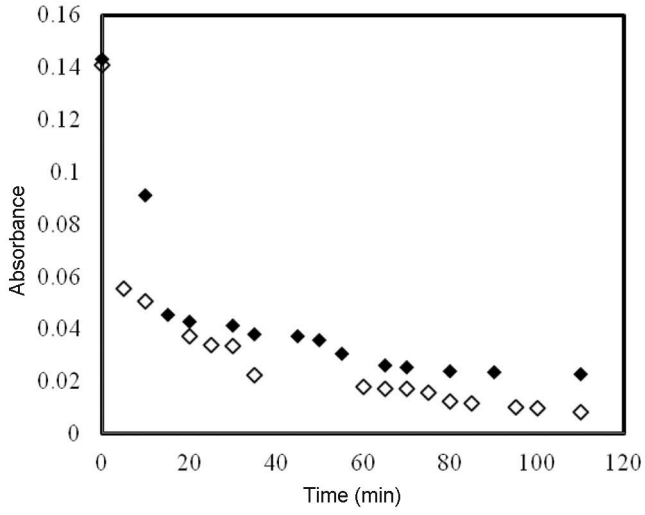

Figure 4. Electrochemical bleaching of RNO in sodium sulphate with different electrodes. (♦) Ti/IrO_2; (◇) $Ti/IrO_2–SnO_2$; current density = 20 mA/cm^2; reaction time = 110 min; pH = 6.14.

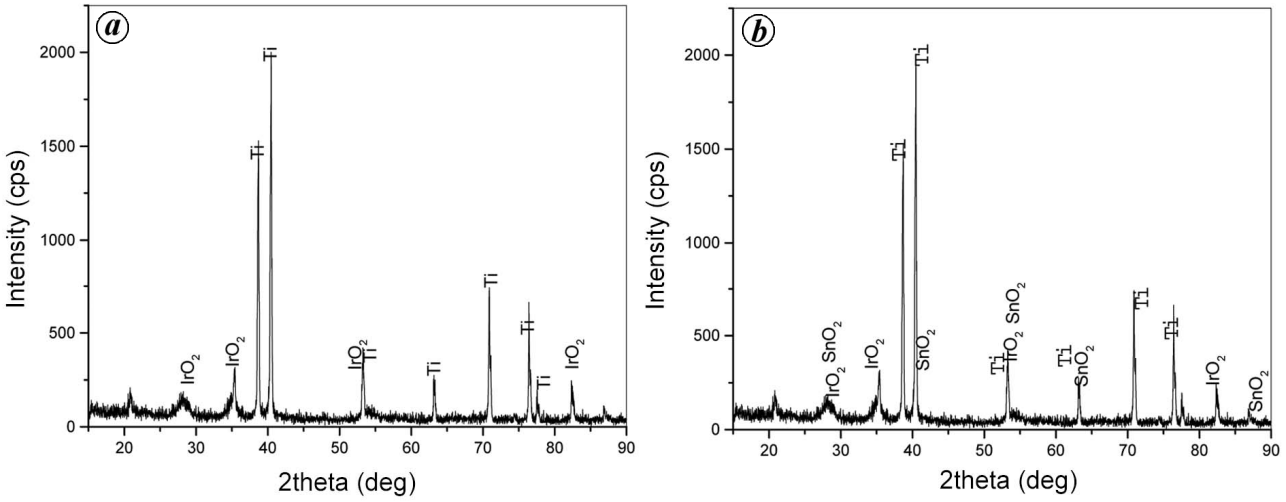

Figure 5. XRD spectra of Ti/IrO_2 anode (***a***) and Ti/IrO_2–SnO_2 anode (***b***).

Mechanism of chlorpyrifos oxidation

The electrochemical oxidation of all organic compounds at anode surfaces occurs due to two states of active oxygen[18]. Physisorbed active oxygen ($MO_x(OH^{\bullet})$), which is adsorbed hydroxyl radical by electrolysis of water, causes the complete combustion of organics (eqs (4) and (6)). Chemisorbed active oxygen (MO_{x+1}), which has oxygen in the oxide lattice (eqs (5) and (7)), is the second type of active oxygen species present at oxide anodes.

$$H_2O + MO_x \rightarrow MO_x(OH^{\bullet}) + H^+ + e^-, \quad (4)$$

$$MO_x(OH^{\bullet}) \rightarrow MO_{x+1} + H^+ + e^-, \quad (5)$$

$$R + MO_x(OH^{\bullet}) \rightarrow CO_2 + zH^+ze + MO_x, \quad (6)$$

$$R + MO_{x+1} \rightarrow RO + MO_x. \quad (7)$$

In this study, the physisorbed active oxygen could be generated by Ti/IrO_2–SnO_2 anode for the electrochemical degradation of chlorpyrifos since its stability is relatively high. Therefore, the rate of degradation of chlorpyrifos is more rapid with Ti/IrO_2–SnO_2 anode than Ti/IrO_2 anode. Chemisorbed active oxygen may be predominant for the degradation at Ti/IrO_2 anode. Similar suggestions have been reported in the literature[31].

Physical characterization

In order to know the phase compositions of the coatings, XRD analysis was conducted. Figure 5 *a* shows the typical X-ray diffractogram obtained for the Ti/IrO_2 anode and Figure 5 *b* shows the X-ray diffractogram obtained for the Ti/IrO_2–SnO_2 anode. The diffractograms revealed characteristic peaks related to the substrate and well-defined peaks for the layer, characterizing a crystalline structure. The XRD data for the main peaks observed in the diffractograms were compared with XRD data from JCPDS (Joint Committee of Powder Diffraction Standards). As can be observed from Figure 5 *a*, characteristic peaks corresponding to IrO_2 were fairly narrow and strong, which is assigned to a rutile crystal structure. In the case of Ti/IrO_2–SnO_2 anode, single peaks were observed at the 110 and 220 phases ($2\theta = 28°$ and 56° respectively), which suggests that it is a solid solution of IrO_2 and SnO_2. Similar observations have been reported in the literature[32]. However, no evidence of metallic phase (Ir and Sn) was observed in both cases. Moreover, diffraction peaks corresponding to the Ti substrate were observed in both anodes, but TiO_2 was not detected.

Voltammetric behaviour and service life of different anodes

Figure 6 shows the CV diagrams obtained for the Ti/IrO_2 and Ti/IrO_2–SnO_2 anodes and uncoated electrode. The CV diagrams showed that the anodic charge increased from 29.8 to 153.76 mC after the development of Ti/IrO_2 anode. In contrast, the anodic charge of Ti/IrO_2–SnO_2 anode was 145.15 mC, resulting in a slightly low electrochemically active surface area than Ti/IrO_2 anode. However, it was observed that both anodes had significantly increased the anodic charge after applying the coating layer compared to the uncoated electrode. The higher anodic charges of coated anodes imply higher electrochemically active surface areas of coated anodes than uncoated electrode. This is important in generating a higher amount of $OH^{\bullet}$ radicals to degrade more chlorpyrifos molecules. However, the decrease of anodic charge of Ti/IrO_2–SnO_2 anode does not imply that it has a lower efficiency than Ti/IrO_2. The better degradation efficiency of the Ti/IrO_2–SnO_2 anode may be due to its catalytic activity, provided by SnO_2.

Accelerated lifetime tests

From a practical point of view, it is important to consider electrochemical stability of the coatings in order to evaluate the efficiency of any electrode. The electrochemical stability of the coatings was evaluated by performing accelerated lifetime test. Figure 7 shows the accelerated lifetime of Ti/IrO_2 and Ti/IrO_2–SnO_2 anodes at a current density of 800 mA cm^{-2} in 0.5 M of H_2SO_4 solution. The figure shows that the accelerated lifetime of the Ti/IrO_2 anode is 7840 sec (approx. 2 h). Interestingly, the accelerated lifetime of Ti/IrO_2–SnO_2 anode is as high as 32,310 sec (538.5 min/approx. 9 h), indicating that it has a more stable layer. The significant increase in the lifetime of Ti/IrO_2–SnO_2 anode is attributed to improvement in stability due to the presence of SnO_2 in the anode. Further, the long lifetime of Ti/IrO_2–SnO_2 anode suggests its cost-effectiveness.

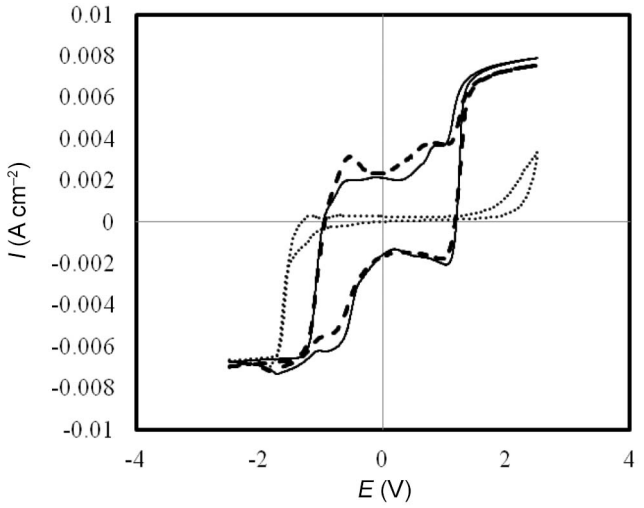

Figure 6. Cyclic voltammograms of Ti/IrO_2 anode (—), Ti/IrO_2–SnO_2 anode (----) and uncoated Ti substrate (····). Scan range = 2.5 to –2.5 V, scan rate = 0.1 V; electrolyte = 0.5 M of Na_2SO_4; and reference electrode is Ag/AgCl.

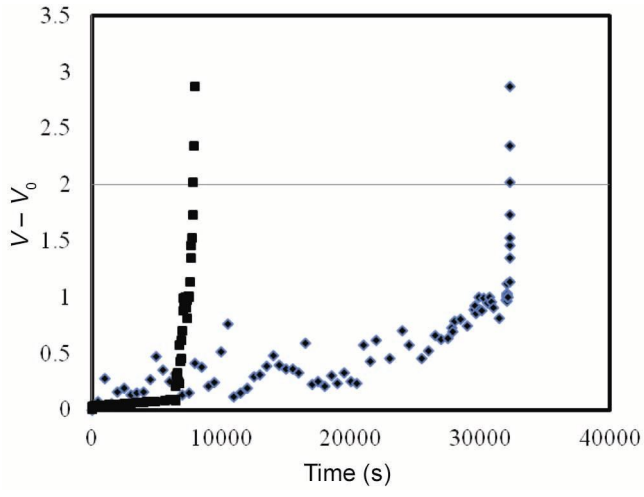

Figure 7. Accelerated lifetime of Ti/IrO_2 anode (■) and Ti/IrO_2–SnO_2 anode (♦). Electrolyte = 0.5 M of Na_2SO_4; current density = 800 mA cm^{-2} and reference electrode is Ag/AgCl.

Figure 8 *a* shows the Atomic Force Microscopic (AFM) image of Ti/IrO_2–SnO_2 anode. It displays a micro-porous, uniform, island-like structure. The dark zones are speculated as IrO_2 with comparatively low surface area, while other region is attributed with SnO_2 (ref. 33). Figure 8 *b* shows the AFM image of Ti/IrO_2–SnO_2 anode after the accelerated lifetime test. Here, R_a is defined as mean roughness, while R_{max} is the vertical distance between the highest and lowest points of the topographic profile. The larger the R_a value, the rougher the surface. It can be seen that the surface of Ti/IrO_2–SnO_2 anode is rough after using it (Table 2). Moreover, it indicates that the coating layer appears as damaged due to failure from protection against passivation. It forms a passive layer, resulting in the formation of an insulating titanium oxide layer due to the oxidation of the titanium substrate[34].

For multilayer metal oxide anodes, the interlayer is the key factor connecting with the Ti substrate to prevent the deactivation of an electrode. In the case of Ti/IrO_2–SnO_2 anode, polymeric precursor offers more agglomerated coating, which leads to delay in the formation of non-conducive TiO_2 layer. Therefore, it can be concluded that the lifetime of the Ti/IrO_2–SnO_2 anode is higher than that of the Ti/IrO_2 anode.

Conclusions

In this article, Ti/IrO_2 and Ti/IrO_2–SnO_2 anodes have been developed for anodic oxidation of chlorpyrifos in a chloride-free environment. The results reveal the following:

- The complete mineralization of chlorpyrifos was not achieved in this study, observing that the prepared Ti/IrO_2–SnO_2 electrode has 78.2% COD removal efficiency in comparison to 65.1% of COD removal efficiency obtained with Ti/IrO_2 electrode after the electrolysis time of 6 h.
- Evolution of COD has followed pseudo second-order kinetics.
- ICE value is always high in Ti/IrO_2–SnO_2 electrode during the period of reaction under similar conditions than the Ti/IrO_2 electrode.

Table 2. Roughness parameters determined by AFM images

Electrode	R_a (nm)	R_{max} (nm)
Fresh Ti/IrO_2–SnO_2	90.016	416.732
Used Ti/IrO_2–SnO_2	122.997	789.294

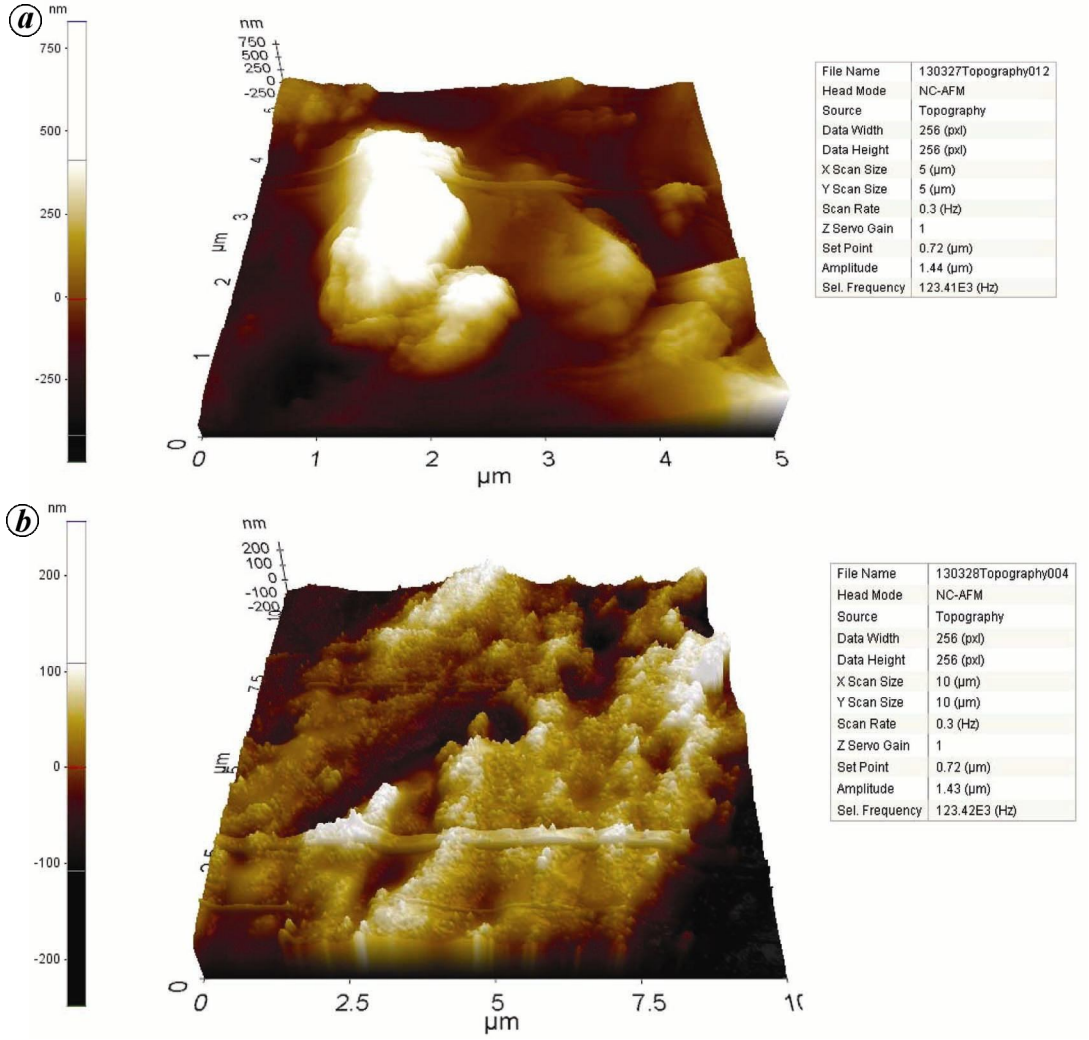

Figure 8. Three-dimensional AFM images of Ti/IrO_2–SnO_2 anode (***a***) before and (***b***) after being used for accelerated lifetime test.

- The hydroxyl radical is the major factor during electrolysis in a chloride-free environment by UV–visible spectrophotometer using RNO and radical scavenging effect.
- CV diagrams show that the anodic charge increases from 29.8 to 153.76 mC for Ti/IrO_2 anode and to 145.15 mC for Ti/IrO_2–SnO_2 anode. However, the decrease of anodic charge of Ti/IrO_2–SnO_2 anode does not imply that it has lower efficiency. The efficiency may be relatively better due to its catalytic activity, provided by SnO_2.
- The Ti/IrO_2 anode shows an accelerated lifetime of 7840 sec (approx. 131 min/2 h), while Ti/IrO_2–SnO_2 anode shows 32,310 sec (538.5 min/approx. 9 h), indicating that it has a more stable layer.

The results obtained from the present study indicate that Ti/IrO_2 and Ti/IrO_2–SnO_2 anodes can be successfully used for the treatment of effluents contaminated with chlorpyrifos in a chlorine-free environment.

1. Tang, T., Dong, J., Ai, S., Qiu, Y. and Han, R., Electro-enzymatic degradation of chlorpyrifos by immobilized hemoglobin. *J. Hazard. Mater.*, 2011, **188**, 92–97.
2. Claver, A., Ormad, P., Luisguez, R. and Ovelleiro, L., Study of the presence of pesticides in surface waters in the Ebro river basin (Spain). *Chemosphere*, 2006, **64**, 1437–1443.
3. Jergentz, S., Mugni, H., Bonetto, C. and Schulz, R., Assessment of insecticide contamination in runoff and stream water of small agricultural streams in the main soybean area of Argentina. *Chemosphere*, 2005, **61**, 817–826.
4. Menon, P., Gopal, M. and Parsad, R., Effects of chlorpyrifos and quinalphos on dehydrogenase activities and reduction of Fe^{3+} in the soils of two semi-arid fields of tropical India. *Agricult. Ecosys. Environ.*, 2005, **108**, 73–83.
5. World Health Organization, Chlorpyrifos in drinking-water. Background document for preparation of WHO Guidelines for drinking-water quality, 2003; (WHO/SDE/WSH/03.04/87) http://www.who.int/water_sanitation_health/dwq/chemicals/chlorpyrifos.pdf; (accessed December 2012).
6. US Environmental Protection Agency, Drinking water assessment of chlorpyrifos. Pesticides and toxic substances. Office of Prevention, Washington, DC, 1998; http://www.epa.gov/oppsrrd1/REDs/chlorpyrifos_red.pdf (accessed December 2012).

7. Mallick, K., Bharati, K., Banerji, A., Shakil, N. A. and Sethunathan, N., Bacterial degradation of chlorpyrifos in pure cultures and in soil. *Bull. Environ. Contam. Toxicol*., 1999, **62**, 48–54.
8. Murillo, R., Sarasa, J., Lanao, M. and Ovelleiro, J. L., Degradation of chlorpyriphos in water by advanced oxidation processes. *Wat. Sci. Technol.: Water Supply*, 2010, **10**, 1–6; doi: 10.2166/ws.2010.777.
9. Devi, L. G., Murthy, B. N. and Kumar, S. G., Photocatalytic activity of V^{5+}, Mo^{6+} and Th^{4+} doped polycrystalline TiO_2 for the degradation of chlorpyrifos under UV/solar light. *J. Mol. Catal. A: Chem*., 2009, **308**, 174–181.
10. Zhang, Y., Xiao, Z., Chen, F., Ge, Y., Wu, J. and Hu, X., Degradation behavior and products of malathion and chlorpyrifos spiked in apple juice by ultrasonic treatment. *Ultrason. Sonochem*., 2010, **17**, 72–77.
11. Zhang, Y., Hou, Y., Chen, F., Xiao, Z., Zhang, J. and Hu, X., The degradation of chlorpyrifos and diazinon in aqueous solution by ultrasonic irradiation: effect of parameters and degradation pathway. *Chemosphere*, 2011, **82**, 1109–1115.
12. Meiqiang, Y., Tengcai, M., Jialiang, Z., Mingjing, H. and Buzhou, M., The effect of high-pressure arc discharge plasma on the degradation of chlorpyrifos. *Plasma Sci. Technol*., 2006, **8**, 727–731.
13. Mori, M. N., Oikawa, H., Sampa, M. H. O. and Duarte, C. L., Degradation of chlorpyrifos by ionizing radiation. *J. Radioanal. Nucl. Chem*., 2006, **270**, 99–102.
14. Fockedey, E. and Lierde, A. V., Coupling of anodic and cathodic reactions for phenol electro-oxidation using three-dimensional electrodes. *Water Res*., 2002, **36**, 4169–4175.
15. Li, X. Y., Cui, Y. H., Feng, Y. J., Xie Z. M. and Gu, J. D., Reaction pathways and mechanisms of the electrochemical degradation of phenol on different electrodes. *Water Res*., 2005, **39**, 1972–1981.
16. Martínez-Huitle, C. A. and Andrade, L. S., Electrocatalysis in wastewater treatment: recent mechanism advances. *Quim. Nova*, 2011, **34**, 850–858.
17. Chen, G., Electrochemical technologies in wastewater treatment. *Sep. Purif. Technol*., 2004, **38**, 11–41.
18. Comninellis, C., Electrolysis in the electrochemical conversion/combustion of organic pollutants for waste water treatment. *Electrochim. Acta*, 1994, **39**(11–12), 1857–1862.
19. Song, S., Zhan, L., He, Z., Lin, L., Tu, J. and Zhang, Z., Mechanism of the anodic oxidation of 4-chloro-3-methyl phenol in aqueous solution using Ti/SnO_2–Sb/PbO_2 electrodes. *J. Hazard. Mater*., 2010, **175**, 614–621.
20. Zheng, Y., Su, W., Chen, S., Wu, X. and Chen, X., Ti/SnO_2–Sb_2O_5–RuO_2/α–PbO_2/β-PbO_2 electrodes for pollutants degradation. *Chem. Eng. J*., 2011, **174**, 304–309.
21. Zhu, X., Ni, J., Wei, J., Xing, X., Li, H. and Jiang, Y., Scale-up of BDD anode system for electrochemical oxidation of phenol simulated wastewater in continuous mode. *J. Hazard. Mater*., 2010, **184**, 493–498.
22. Samet, Y., Agengui, L. and Abdelhédi, R., Anodic oxidation of chlorpyrifos in aqueous solution at lead dioxide electrodes. *J. Electroanal. Chem*., 2010, **650**, 152–158.
23. Tian, M., Bakovic, L. and Chen, A., Kinetics of the electrochemical oxidation of 2-nitrophenol and 4-nitrophenol studied by *in situ* UV spectroscopy and chemometrics. *Electrochim. Acta*, 2007, **52**, 6517–6524.
24. Clesceri, L. S., Greenberg, A. E. and Eaton, A. D., *Standard Methods for the Examination of Water and Wastewater*, United Book Press, USA, 1998, 18th edn.
25. Sun, H., Lin, H., Du, L., Huang, W., Li, H. and Cui, T., Electrochemical oxidation of aqueous phenol at low concentration using Ti/BDD electrode. *Sep. Purif. Technol*., 2012, **88**, 16–120.
26. Li, M., Feng, C., Hu, W., Zhang, Z. and Sugiura, N., Electrochemical degradation of phenol using electrodes Ti/RuO_2–Pt and Ti/IrO_2–Pt. *J. Hazard. Mater*., 2009, **162**, 455–462.
27. Deng, Y. and Englehardt, J. D., Electrochemical oxidation for landfill leachate treatment. *Waste Manage*., 2007, **27**, 380–388.
28. Moraes, P. B. and Bertazzoli, R., Electrodegradation of landfill leachate in a flow electrochemical reactor. *Chemosphere*., 2005, **58**, 41–46.
29. Wu, D., Liu, M., Dong, D. and Zhou, X., Effects of some factors during electrochemical degradation of phenol by hydroxyl radicals. *Microchem. J*., 2007, **85**, 250–256.
30. Polcaro, A. M., Palmas, S., Renoldi, F. and Mascia, M., On the performance of Ti/SnO_2 and Ti/PbO_2 anodes in electrochemical degradation of 2-chlorophenol for waste water treatment. *J. Appl. Electrochem*., 1999, **29**, 147–151.
31. Wang, Y., Gua, B. and Xua, W., Electro-catalytic degradation of phenol on several metal-oxide anodes. *J. Hazard. Mater*., 2009, **162**, 1159–1164.
32. Mayousse, E., Maillard, F., Fouda-Onana, F., Sicardy, O. and Guillet, N., Synthesis and characterization of electrocatalysts for the oxygen evolution in PEM water electrolysis. *Int. J. Hydrogen Energy*, 2011, **36**, 10474–10481.
33. Mussy, J. P. G. D., Macpherson, J. V. and Delplancke, J. L., Characterization and behavior of Ti/TiO_2/noble metal anodes. *Electrochim. Acta*, 2003, **48**, 1131–1141.
34. Chen, Y., Hong, L., Xue, H., Han, W., Wang, L., Sun, X. and Li, J., Preparation and characterization of TiO_2–NTs/SnO_2–Sb electrodes by electrodeposition. *J. Electroanal. Chem*., 2010, **648**, 119–127.

ACKNOWLEDGEMENT. We thank the National Research Council, Sri Lanka (grant no: 11-054), for financial support.

Received 20 September 2013; revised accepted 19 May 2014